Nanoscale

Accepted Manuscript

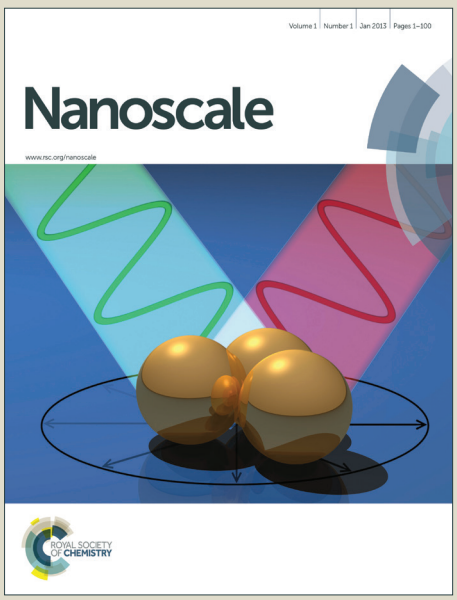

ROYAL SOCIETY OF CHEMISTRY

www.rsc.org/nanoscale

Theranostic probe for simultaneous *in vivo* photoacoustic imaging and confined photothermolysis by pulsed laser at 1064 nm in 4T1 breast cancer model

Min Zhou,[a] Geng Ku,[a] Laura Pageon[b] and Chun Li *[a]

[a]Department of Cancer Systems Imaging, The University of Texas MD Anderson Cancer Center, Houston, Texas 77030 U.S.A E-mail: cli@mdanderson.org; Tel: +1 713 792 5182

[b]Department of Veterinary Medicine & Surgery, The University of Texas MD Anderson Cancer Center, Houston, Texas 77030 U.S.A.

***Corresponding Author:** Chun Li, Department of Cancer Systems Imaging, Unit 1907, The University of Texas MD Anderson Cancer Center, Houston, Texas 77030; Tel: 713-792-5182; Fax: 713-794-5456; E-mail: cli@mdanderson.org.

Abstract

Here, we report that polyethylene glycol (PEG)-coated copper(II) sulfide nanoparticles (PEG-CuS NPs) with their peak absorption tuned to 1064 nm could be used both as a contrast agent for photoacoustic tomographic imaging of mouse tumor vasculature and as a mediator for confined phothermolysis of tumor cells in an orthotopic syngeneic 4T1 breast tumor model. PEG-CuS NPs showed stronger photoacoustic signal than hollow gold nanospheres and single-wall carbon nanotubes at 1064 nm. MicroPET imaging of 4T1 tumor-bearing mice showed a gradual accumulation of the NPs in the tumor over time. About 6.5% of injected dose were taken up in each gram of tumor tissue at 24 h after intravenous injection of ^{64}Cu-labeled PEG-CuS NPs. For both photoacoustic imaging and therapeutic studies, nanosecond (ns)-pulsed laser was delivered with Q-switched Nd:YAG at a wavelength of 1064 nm. Unlike conventional photothermal ablation therapy mediated by continuous wave laser with which heat could spread to the surrounding normal tissue, interaction of CuS NPs with short pulsed laser deliver heat rapidly to the treatment volume keeping the thermal damage confined to the target tissues. Our data demonstrated that it is possible to use a single-compartment nanoplatform to achieve both photoacoustic tomography and highly selective tumor destruction at 1064 nm in small animals.

1. Introduction

Advances in photoacoustic tomography (PAT), which is based on nonradiative conversion of adsorbed photothermal energy to acoustic signal, have demonstrated promising potential in biomedical applications.[1-3] PAT can be enhanced either by using endogenous biomolecules as natural PAT contrast agents or by using exogenous compounds as PAT contrast agents. Various exogenous agents have been shown to be efficient contrast agents for PAT, including gold nanomaterials,[4-9] carbon-based nanoparticles (NPs),[10-12] and CuS NPs.[13] Advantages of NPs include their higher optical absorption, photostability, and favorable tumor accumulation due to the enhanced permeability and retention effect. [7,14]

CuS NPs, a new class of PAT contrast and photothermal conducting agents, display strong absorption peaks in the near-infrared (NIR) region (~900-1100 nm) [13,15,16] CuS NPs are much smaller (diameter < 15 nm) than plasmonic Au nanostructures that absorb NIR light, and thus CuS NPs more easily extravasate from the tumor blood vessels and have a better chance of reaching their targets.[16] CuS NPs have shown promise as contrast agents for PAT of mouse brain and rat lymph nodes because CuS NPs offer high resolution and allow deep tissue penetration.[13]

Here, we report that CuS NPs with their peak absorption tuned to 1064 nm could be used both as a contrast agent for PAT of mouse tumor vasculature and as a mediator for confined photothermolysis destruction of tumor cells in an orthotopic mouse breast tumor model. Q-switched Nd:YAG laser, which emits light at a primary wavelength of 1064 nm, is one of the most reliable light sources for PAT.[13,17] More stable photoacoustic signal can be acquired at 1064 nm than at other wavelengths because of greater fluence rate achievable at 1064 nm. Furthermore, the background photoacoustic signal from

tissue is relatively low at 1064 nm, which represents the second optical window for low background signal and high signal-to-background ratio with the use of contrast agent.[17]

2. Experimental

2.1. Reagents

Copper(II) chloride ($CuCl_2$), sodium sulfide ($Na_2S \cdot 9H_2O$), and methoxy-PEG-thiol (PEG-SH, molecular weight 5000) were purchased from Sigma-Aldrich (St. Louis, MO, USA). Hollow gold nanoshells (HAuNS) were prepared according to a previously reported method.[6] Single-wall carbon nanotubes (SWNTs) were purchased from Nanostructured & Amorphous Materials, Inc. (Houston, TX, USA). Isoflurane was purchased from Baxter (Deerfield, IL, USA).

2.2. General procedure for the synthesis of PEG-CuS Nanoparticles (NPs)

Into 100 mL of an aqueous solution of $CuCl_2$ (0.1 mmol) and PEG-SH (0.2 mmol) was added 0.1 mL of sodium sulfide solution (Na_2S, 1 M) under stirring at room temperature. Five minutes later, the reaction mixture was heated to 90°C and stirred at 1000 rpm for 15 min until a dark green solution was obtained. NPs with peak absorption at 1064 nm were obtained by adjusting the stoichiometric ratio between $CuCl_2$ and Na_2S. Free $CuCl_2$, PEG-SH and Na_2S were removed by a ultra-centrifugal filter unit (Amicon Ultra-15, 50 kDa, Billerica, MA, USA).

2.3. Characterization of PEG-CuS NPs

For transmission electron microscopy, an aqueous solution of PEG-CuS NPs was deposited on carbon-enhanced copper grids without negative staining. The NPs were allowed to adhere on the grid for 1 h, after which they were briefly rinsed with deionized

water and air-dried. The samples were then examined using a transmission electron microscope (JEM 2010, JEOL Japan) at an accelerating voltage of 200 kV. Digital images were obtained using the AMT Imaging System (Advanced Microscopy Techniques Corp., Danvers, MA, USA). The extinction spectrum of the NPs was measured using a UV-Vis spectrophotometer (DU 800, Beckman Coulter, Inc., Brea, CA, USA). The fraction of incident light transmitted through a solution of NPs was recorded, and then the extinction coefficient was derived according to energy conservation.

2.4. Photoacoustic imaging of gel cylinders embedded in chicken breast tissue

To investigate the photoacoustic signal of various nanomaterials, various gel cylinders (5 mm in diameter × 4 mm in length) were embedded in a piece of chicken breast muscle of ~9 cm in diameter. Six gel objects were obtained by mixing 2% agarose with PEG-CuS NPs, HAuNS, and SWNTs at concentrations of 100 μg/mL and 20 μg/mL. One gel object without nanomaterials was prepared as a reference. The piece of chicken breast muscle containing the embedded gel cylinders was placed under 1 piece of 1-cm thick chicken breast muscle. Laser light was used to illuminate the chicken breast muscle from above, and the photoacoustic signals emitted from the embedded gel objects were detected by the circularly scanning transducers. The data were reconstructed using a back-projection algorithm. The intensity of the light that transmitted through various tissue depths was determined using a photodiode detector (DET110, Thorlabs, Newton, NJ, USA).

2.5. PAT of blood vascular structures of 4T1 breast cancer

All experiments involving animals were approved by the Institutional Animal Care and Use Committee (IACUC). Female Balb C mice (Charles River Laboratories, Wilmington,

MA, USA) were inoculated orthotopically with 5×10^6 4T1 cells in the upper right mammary fat pads (n = 3). Imaging and therapy studies were performed when tumors had grown to 5-10 mm in diameter (~2 weeks after inoculation). For the in vivo PAT experiment, Balb C mice were anesthetized using veterinary anesthesia equipment (Mobile 901807, VetEquip, Pleasanton, CA, USA) that delivered 2% isoflurane in oxygen at a flow rate of 2 L/min. Laser light was used to illuminate the animal tumor from above, and an ultrasonic detector was used to scan the mouse in its horizontal plane. PEG-CuS NPs (3×10^{13} NP/mL, 1 mM, 100 μg/mL, 2 OD at 1064 nm) in 200 μL of saline were injected intravenously (i.v.) into the mice. PAT imaging was performed at 5 min and 2 h after NPs injection. Tumor excision and fixation proceeded immediately after imaging and euthanasia. Histological evaluation was conducted by means of hematoxylin/eosin and copper staining of paraffin-embedded tissue sections to assess the distribution of PEG-CuS NPs.

2.6. In vitro photothermolysis against 4T1 breast cancer cells

4T1 breast cancer cells were seeded onto a 24-well plate with a density of 50,000 cells per well 1 day before the experiment. Cells were washed 3 times with Hank's balanced salt solution (HBSS, Sigma-Aldrich) and then incubated with PEG-CuS NPs in RPMI-1640 culture medium (Invitrogen, Carlsbad, CA, USA) at a CuS concentration of 100 μg/mL at 37 °C. Cells without NPs were used as a control. After 2 h, the culture medium was replaced with fresh RPMI-1640 medium without phenol red, and the cells were irradiated with a Nd:YAG pulsed 10-ns laser at 1064 nm at an average power density of 1.6 W/cm^2 for 30 s. After treatment, cells were resupplied with RPMI-1640 containing 10% fetal bovine serum. After 24 h, the cells were washed with HBSS and stained with calcein AM and EthD-1 for visualization of viable and dead cells according to the

manufacturer's suggested protocol (Invitrogen). Cells were examined under a Zeiss Axio Observer Z1 fluorescence microscope (Carl Zeiss MicroImaging GmbH, Göttingen, Germany).

2.7. In vivo temperature changes under NIR laser light

For measurement of temperature change mediated by PEG-CuS NPs, continuous NIR laser light (808 nm, 3 W/cm^2, Diomed, Andover, MA) or pulse laser light (1064 nm, 4.32 W/cm^2) was delivered to the 4T1 tumors in mice 24 h after i.v. injection of PEG-CuS NPs (200 μL, 2 OD). Thermographic pictures were taken by means of a thermal camera (Flir i7, Flir Systems Inc., Portland, USA).

2.8. In vivo photothermolysis therapy against 4T1 breast cancer

For the in vivo photothermolysis experiment, mice bearing 4T1 breast tumors (5−7 mm in diameter) were randomly allocated into 3 groups consisting of 4 mice each. Mice in group A were injected i.v. with PEG-CuS NPs (200 μL, 2 OD) in 200 μL of saline. Mice in groups B and C were injected i.v. with saline. Twenty-four hours after NPs or saline injection, the animals were anesthetized, and the mice in groups A and B were irradiated with the 1064-nm pulsed laser at an average power density of 4.32 W/cm^2 for 30 s (10 pulses/second, spot size 0.4 cm in diameter). Mice in group C were not treated with laser and were used as a control. All the mice were killed 24 h after laser treatment, and tumors were removed and processed for histologic evaluation. One histological section was obtained from each tumor specimen and stained with hematoxylin and eosin. The sections were examined by a board-certified veterinary pathologist (LP) and histopathologic changes were recorded. For estimation of the extent of overall tissue necrosis and viable tumor size, one slice representing the whole tumor with overlying

subcutaneous tissue and haired skin was evaluated. Percentages of necrosis and extent of tumor viability were based on subjective visual estimates of these features in the histological sections.

3. Results and Discussion

The absorption peak of CuS NPs was tuned to 1064 nm by adjusting the stoichiometric ratio between the 2 reactants, $CuCl_2$ and Na_2S in the presence of sulfhydryl methoxy-polyethylene glycol (PEG-SH). The major difference between PEG-CuS NPs used in the current study and PEG-CuS NPs reported in previous studies was further red-shift of the absorption peak from 930-990 nm to 1064 nm.[13,16] **Figure 1A** shows a typical extinction spectrum for PEG-CuS NPs in aqueous solution with concentration equivalent to 100 μg/mL CuS molecules. The absorption peak is around 1064 nm. Matching peak absorption of NPs to the designated wavelengths of the laser light is expected to increase the efficacy of both PAT signal and laser treatment. Moreover, PEG-CuS NPs have high colloidal stability. The size of PEG-CuS NPs in aqueous solution remained unchanged after 6 months of storage at 4°C in the presence of argon (see the inset of **Fig. 1A** and **Fig. S1**). The stability of PEG-CuS NPs was further investigated by incubating these NPs in physiological media, including phosphate-buffered saline (PBS) and PBS containing 10% fetal bovine serum (FBS) at 37 °C for up to 7 days. No obvious changes in UV-Vis spectra were found during the incubation period (Supporting Information, **Figure S2**), indicating that PEG-CuS NPs possess excellent colloidal stability. **Figure 1B** is a transmission electron microscopy photograph of the type of PEG-CuS NPs employed in our study. On the basis of transmission electron microscopy, the mean diameter of the PEG-CuS NPs core was ~17 nm, which was slightly larger than PEG-CuS NPs with peak absorption of 990 nm

(~11 nm). **Figure 1C** shows the distribution of hydrodynamic diameters of PEG-CuS NPs determined using dynamic light scattering analysis. The mean hydrodynamic diameter was 35.8 nm because of the hydrophilic PEG coating present on the CuS NPs surface.

Other nanomaterials have also been proposed as contrast agents for in vivo PAT, including hollow gold nanoshells (HAuNS)[6,7] and single-wall carbon nanotubes (SWNTs).[11] However, these agents have low absorption at 1064 nm. **Figure 2A** compares the optical extinction spectra of PEG-CuS NPs, HAuNS, and SWNTs. At 1064 nm, PEG-CuS NPs displayed an optical extinction value (OD = 2.19) more than twice that of HAuNS (OD = 0.83) and ~7 times that of SWNTs (OD = 0.31) at measured the same concentration of 100 μg/mL. Giving that optical extinction is based on absorption and scattering and that scattering signal is proportional to NP size according to Mie's theory, the difference in absorbance between PEG-CuS NPs, HAuNS, and SWNTs would be even greater.

We then compared the performance of PEG-CuS NPs, HAuNS, and SWNTs in PAT acquired at a wavelength of 1064 nm. Agarose gels containing PEG-CuS NPs, HAuNS, and SWNTs were embedded in a piece of chicken breast muscle, which was then placed under a piece of 1-cm-thick chicken breast muscle (**Fig. 2B**). **Figure 2C** shows PAT images obtained at a depth of 1 cm. The agarose gel containing 100 μg/mL PEG-CuS NPs was clearly visualized. The agarose gel containing 100 μg/mL HAuNS was also visualized, albeit at much lower signal intensity. No signal of SWNTs could be seen at the concentration of 100 μg/mL. At a concentration of 20 μg/mL, only PEG-CuS NPs were visualized (**Fig. 2C**). These data indicate that PEG-CuS NPs had greater photoacoustic signal than HAuNS and SWNTs and that PEG-CuS NPs are well suited as a contrast agent for in vivo PAT at 1064 nm.

Representative micro-PET/CT images of a 4T1-tumor bearing mouse acquired at 10 min, 2 h, and 24 h after i.v. injection of PEG-[^{64}Cu]CuS NPs revealed high uptake of PEG-[^{64}Cu]CuS NPs in the liver and spleen. As expected, PEG-[^{64}Cu]CuS NPs gradually accumulated in the tumor between 10 min and 24 h, permitting clear visualization of the tumor 24 h after injection (**Fig. 3A**). PEG-[^{64}Cu]CuS NPs were distributed to and retained in the tumor over the 24 h period, possibly as a result of enhanced permeability and retention effect. Biodistribution data obtained at 24 h after i.v. injection of PEG-[^{64}Cu]CuS NPs are consistent with the micro-PET/CT imaging findings (**Fig. 3B**). Results show that liver had the highest uptake of the NPs (25.8 ± 3.3 %ID/g). Interestingly, the tumor uptake of PEG-[^{64}Cu]CuS NPs reached 6.53 ± 1.85 %ID/g, which was higher than their accumulation in the other major organs (spleen: 4.34 ± 0.69 %ID/g; kidney: 3.97 ± 0.88 %ID/g).

Next, we investigated the capacity of PEG-CuS NPs as a contrast agent for PAT imaging of 4T1 tumors. The blood vessel network of a tumor not only regulates the supply of nutrients and oxygen to the cancer cells, which affects their survival and growth, but also influences the response of the tumor to therapy.[18,19] Noninvasive in vivo study of the tumor blood vasculature is therefore of interest in fundamental cancer research and the development of new drugs and other therapies. **Figure 4A** is a representative in vivo PAT image of the blood vessel structure of an orthotopic mouse 4T1 breast tumor acquired at 1064 nm without contrast agent. Several large vessels can be seen possible because of the light absorption of the hemoglobin and water. However, smaller blood vessels are not discernible. At 5 min and 2 h after i.v. administration of PEG-CuS NPs (200 μL, 100 μg/mL, 2 OD), blood vessel structures, including smaller vessels, were more clearly visualized (**Fig. 4B and 4C**). Moreover, the corresponding photoacoustic signals had more intensified peaks and nadirs after contrast agent

injection (**Fig. 4D-F**), indicating increased tissue contrast after NP injection. These results suggest that the 1064-nm PEG-CuS NPs are a promising contrast agent for PAT of tumor blood vessels.

Histological examination of tumors using copper staining confirmed the presence of copper in the tumors of mice treated with PEG-CuS NPs (**Supporting Information Fig. S3**), indicating significant tumor accumulation of CuS NPs.

To investigate the cell killing induced by pulsed laser at 1064 nm, we incubated 4T1 murine breast cancer cells with PEG-CuS NPs (100 μg/mL) for 2 h. The cells were then irradiated with ns-pulsed laser at 1064 nm at an average power density of 1.6 W/cm^2 for 30 s. Cell viability after exposure to the laser was examined using calcein AM dye, which reports ubiquitous intracellular esterase activity. At 24 h after laser treatment, no live cells were seen in the laser-exposed area (**Fig. 5A**). However, there was no apparent change in cell viability when 4T1 cells were treated with PEG-CuS NPs alone (100 μg/mL) or ns-pulsed laser alone at the same laser dose (**Fig. 5B and 4C**). These results indicated that PEG-CuS NPs mediated efficient destruction of 4T1 cells.

Supporting Information Figure S4 shows the temperature change of an aqueous solution of PEG-CuS NPs (100 μg/mL) as a function of exposure time. Exposure of the solution to continuous wave 808-nm laser light at 3 W/cm^2 for 30 s elevated the temperature of the solution from 22 °C to 43 °C (ΔT = 21 °C). However, the change in temperature with 1064-nm pulsed laser at 4.32 W/cm^2 was moderate, from 22 °C to 29 °C (ΔT = 7 °C), even though the absorbance at 1064 nm was more than 2 times greater than at 808 nm (2.19 OD vs. 0.92 OD). No significant change in temperature was observed when pure water was irradiated with 1064-nm pulsed laser under the same conditions. **Figure 6** shows infrared thermographic images of 4T1 tumor-bearing mice with and without i.v. injection of PEG-CuS NPs, followed by irradiation at 1064-nm (at

4.32 W/cm^2) with pulsed laser or at 808 nm (at 3 W/cm^2) with continuous wave laser light for 2 min. The temperature of the tumors treated with continuous wave laser was elevated above 50 °C (ΔT = 20.7 °C), while the temperature of the tumors treated with pulsed laser only increased 6.8 °C. It is anticipated that the temperature elevation after exposure to a continuous wave laser at 1064 nm would have been greater than observed at 808 nm because PEG-CuS NPs had much stronger absorption at 1064 nm than at 808 nm (**Fig. 1A**). These data are consistent with the hypothesis that cell death caused by exposure of PEG-CuS NP-treated tumor cells to pulsed laser is mediated by a highly confined thermolysis phenomenon that probably involves both heat and mechanical (acoustic) destruction throughout the treatment volume. Anderson and Parrish[20] were the first to describe selective damage to pigmented cells and organelles using endogenous absorbers such as melanin, and further proposed the use of selective absorption of pulsed laser for precise microsurgery. It has been reported that pulsed laser generates photomechanical energy or shock waves to induce nanoscale transient vapor bubbles around photothermal conducting NPs.[21-23] These shock waves or bubbles cause cells to collapse and die. However, it is debatable whether these gaseous “nano-bubbles” truly existed. Clearly, further studies are needed to elucidate the mechanism of cell death caused by interaction between pulsed laser and NIR light-absorbing nanoparticles.

We next evaluated the in vivo therapeutic effect of intravenous injected PEG-CuS NPs with and without laser irradiation. Histologically, orthotopic 4T1 mammary adenocarcinoma was unencapsulated, relatively well-circumscribed, and compressed the surrounding normal tissue (n = 4/group). The tumor infiltrated the subcutaneous tissue and deep dermis focally. In saline-treated control group, each tumor was comprised almost entirely of viable neoplastic cells. There was only a baseline fraction of

necrosis in tumor tissue (<1%, **Fig. S5**). Epidermal tissue was intact (**Fig. 7A**, top panel). The average apoptotic index was 0.4 % and the average mitotic index was 2.3 %. In saline and laser-treated group, each tumor was comprised largely of viable neoplastic cells. Occasionally, small, scattered areas of coagulative/lytic necrosis were evident within these tumors; these foci comprise less than 3% of the tumor mass (**Fig. S5**). Occasional hemorrhage and edema were observed. Epidermal necrosis/ulceration was not present (**Fig. 7A**, middle panel). The average apoptotic index was 0.45 % and the average mitotic index was 2.8 % for this group.

In groups of tumors removed at 4 h and 24 h after treatment with PEG-CuS NPs and laser, tumors demonstrated prominent, confluent areas of coagulative/lytic necrosis that affected approximately 50-75 % of the neoplasm. Coagulative/lytic necrotic foci demonstrated varying morphologic changes characteristic of necrosis including karyolysis (chromatin dissolution/nuclear fading), pyknosis (chromatin clumping/nuclear shrinkage), karyorrhexis (nuclear fragmentation), nuclear dissolution and cytoplasmic clumping. Ablated neoplastic cells were polygonal, non-cohesive, and shrunken. The ablated cells had distinct cell borders and contain hypereosinophilic cytoplasm and hyperchromatic nuclei. Ablated neoplastic cells were often rimmed by moderate hemorrhage, edema and inflammation. Inflammatory infiltrates were composed of moderate numbers of neutrophils and lesser mononuclear cells. Most of the tumors in this group demonstrated epidermal necrosis/ulceration (**Fig. 7A**, bottom panel). The average apoptotic index was 0.55 % and 0.35 % at 4 h and 24 h intervals, respectively, and the average mitotic index was 0.9 % and 1.5% at 4 h and 24 h, respectively. No significant differences in histopathologic findings were noted between the 4 h and the 24 h post-laser treatment specimens.

These data indicate that necrosis rather than apoptosis was the primary cause of cell death induced by short pulsed laser at 1064 nm. It is interesting to note that with 15-ns pulsed laser, the laser ablation zone was confined to a depth of 4-5 mm with clearly defined boundary separating the ablated zone from un-ablated zone (**Fig. 7A**, bottom panel & **7B**). The interface with mixed viable cells and ablated cells is about 100 μm. Thus, confined photothermolysis with pulsed laser differs from other thermal ablation techniques (i.e. radiofrequency, microwave, continuous wave laser-induced thermal therapy) in that ablation zone could be accurately controlled possibly as a result of the absence of heat gradient. In traditional thermal ablation therapy including photothermal ablation therapy with continuous wave laser beam, heat dissipation from the site of action would result in huge variation in ablation zone, making it difficult to apply those techniques to the ablation of tumors adjacent to vital organs.

4. Conclusions

In summary, we have developed a highly efficient, multifunctional theranostic platform for simultaneous PAT and confined photothermolysis suitable for microsurgical applications. With use of a low-cost Nd:YAG laser at a wavelength of 1064 nm for photoacoustic excitation, the blood vasculature of tumors enhanced significantly after administration of PEG-CuS NPs. Furthermore, we showed that the PEG-CuS NPs mediated in vivo photothermolysis ablation at a low laser power density with a promising potential for accurate spatial control of ablation zone. To the best of our knowledge, this is the first report on the use of nanomaterials to mediate simultaneous PAT of tumor vasculature and confined photothermolysis therapy in an orthotopic animal model. Future development of this new class of multifunctional CuS NPs included their targeted

delivery to tumor cells will open exciting opportunities for theranostic biomedical applications.

Acknowledgements

We would like to thank Stephanie P. Deming for editing this manuscript. This research was supported by National Cancer Institute grant U54CA151668 (CL), the John S. Dunn Research Foundation (CL), and the National Cancer Institute through Cancer Center Support Grant CA016672, which supports the Small Animal Imaging Facility and High Resolution Electron Microscopy Facility at MD Anderson Cancer Center.

Electronic Supplementary Information (ESI) available: [details of any supplementary information available should be included here]. See DOI: 10.1039/b000000x/

Supplementary data: details on methods used for copper staining, synthesis of ^{64}Cu-labeled PEG-CuS NPs, and PAT imaging equipment, and data summary on stability of PEG-CuS NPs, photographs of copper staining in tumor samples, temperature elevation comparing continues wave and pulsed laser beams, and quantitative analysis of treatment-induced necrosis of tumor tissues.

.

Figure Captions

Fig. 1. Characterization of CuS NPs. A) Extinction spectra of 100 μg/mL CuS NPs aqueous solution. Inset: photograph of an aqueous solution of PEG-CuS NPs after storage at 4°C for 6 months in the presence of argon. B) Transmission electron microscopy photograph of CuS NPs. Inset: particle size distribution. C) Hydrodynamic diameter distribution of PEG-CuS NP samples determined by dynamic light scattering measurement immediately after synthesis.

Fig. 2. Optical absorbance and visualization on PAT of different PAT contrast agents. A) Optical absorbance of CuS NPs, HAuNS, and SWNTs at the same concentration, 100 μg/mL. B) Photograph, and C) PAT image of agarose gels containing nanomaterials embedded in a piece of chicken breast muscle, which was then placed under a 1-cm block of chicken breast muscle. Two-dimensional PAT image was acquired from the laser-illuminated surface. 1, CuS NPs 100 μg/mL; 2, HAuNS 100 μg/mL; 3, SWNTs 100 μg/mL; 4, CuS NPs 20 μg/mL; 5, HAuNS 20 μg/mL; 6, SWNTs 20 μg/mL; and 7, gel without contrast agent.

Fig. 3. A) Micro-PET/CT images of Blab C mice bearing 4T1 breast cancer acquired at 10 min, 2 h, and 24 h after i.v. injection of PEG-[^{64}Cu]CuS NPs. Yellow arrow, tumor. B) Biodistribution of PEG−CuS NPs (n = 3) at 24 h after i.v. injection in mice bearing 4T1 breast tumor.

Fig. 4. Representative in vivo PAT images of a 4T1 mammary tumor grown in the mammary fatpad and corresponding PA signals (n = 3). Images were acquired using ns-pulsed laser light at a wavelength of 1064 nm A) before CuS NP

injection, B) 5 min after intravenous injection of 200 µL of CuS NP solution (100 µg/mL, 2 OD), and C) 2 h after intravenous injection of 200 µL of CuS NP solution. D-F) PA signals corresponding to the white lines of the respective PA images.

Fig. 5. Fluorescence photomicrographs of 4T1 cancer cells after confined photothermolysis therapy in vitro. A) 4T1 cells were incubated with CuS NPs at a concentration of 100 µg/mL for 2 h and then treated with ns-pulsed laser at 1064 nm at a power density of 1.6 W/cm^2 for 30 s. B) CuS NPs only (no laser). C) Laser treatment only (no CuS NPs). Viable cells were stained green with calcein AM; dead cells were stained red with Ethd-1. Bar, 100 µm.

Fig. 6. Representative *in vivo* infrared thermographic images of 4T1 tumor-bearing mice obtained with or without PEG-CuS NPs followed by irradiation at 1064-nm (at 4.32 W/cm^2) with pulsed laser or at 808 nm (at 3 W/cm^2) with continuous wave laser light for 2 min.

Fig. 7. Representative microphotographs of H&E-stained slices of 4T1 tumors removed 24 h after treatment (n = 4). Laser treatment was instituted with a 15-ns pulsed laser at 1064 nm at an average power density of 4.32 W/cm^2 for 30 s. Drugs (saline or PEG-CuS NP) were injected intravenously 24 before laser exposure. **A**) Saline-treated control mouse (top panel) shows tumor cells infiltrating the deep dermis and subcutaneous tissue. The tumor is highly cellular and necrosis is not evident. At higher magnification (100X), the tissue demonstrates an intact epidermis. Saline and laser-treated mouse (middle panel) shows almost entirely

of viable neoplastic cells. A small area of coagulative/lytic necrosis is evident within this tumor (arrow). These foci comprise less than 25% of the tumor mass in this group of mice. Epidermal necrosis/ulceration is not present. Treatment with PEG-CuS NPs and laser (Bottom panel) shows necrosis and tumor cell ablation in a significant portion of the tumor (>75%). The ablated cells contain hypereosinophilic cytoplasm and hyperchromatic nuclei. Higher magnification demonstrates necrosis and ablated neoplastic cells (**N**) adjacent to viable neoplastic cells (**V**) with a rim of hemorrhage surrounds the necrosis/ablated neoplastic cells. **B**) Microphotographs of a 4T1 tumor treated with PEG-CuS NPs plus laser showing damage to epidermal tissues in laser exposed area (left) but not in the adjacent un-exposed area (top). The sharp boundary separating laser ablated zone and non-ablated zone is clearly visualized (right). Scale bar in 10X images, 1 mm; scale bar in 100X images, 100 μm.

References

1 H. F. Zhang, K. Maslov, G. Stoica and L. H. V. Wang, *Nat. Biotechnol.*, 2006, **24**, 848-851.

2 C. Kim, C F.avazza and L. H. V. Wang, *Chem. Rev.*, 2010, **110**, 2756-2782.

3 L. H. V. Wang and S. Hu, *Science*, 2012, **5**,1458-1462.

4 S. Mallidi, T. Larson, J. Tam, P. Joshi, A. Karpiouk and K. Sokolov, *Nano Lett.*, 2009, **9**, 2825-2831.

5 Q. Zhang, N. Iwakuma, P. Sharma, B. M. Moudgil, C. Wu and J. McNeill, *Nanotechnology*, 2009, **20**, 395102.

6 W. Lu, Q. Huang, K. Geng, X. X. Wen, M. Zhou, D. Guzatov and C. Li, *Biomaterials*, 2010, **31**, 2617-2626.

7 W. Lu, M. P. Melancon, C. Y. Xiong, Q. Huang, A. Elliott, S. L. Song and C. Li, *Cancer Res.*, 2011, **71**, 6116-6121.

8 G. D. Moon, S. W. Choi, X. Cai, W. Y. Li, E. C. Cho and U. Jeong, *J. Am. Chem. Soc.*, 2011, **133**, 4762-4765.

9 P. Wang, H. Liu, P. Hsu, C. Y. Lin, C. R. C. Wang and P. Y. Chen, *J. Biomed. Opt.*, 2012, **17**, 061222

10 A. De la Zerda, Z. Liu, S. Bodapati, R. Teed, S. Vaithilingam, B. T. Khuri-Yakub and S. Gambhir, *Nano Lett.*, 2010, **10**, 2168-2172.

11 L. Xiang, Y. Yuan, D. Xing, Z. Ou, S. Yang and F. Zhou, *J. Biomed. Opt.*, 2009, **14**, 021008.

12 A. De la Zerda, C. Zavaleta, S. Keren, S. Vaithilingam, S. Bodapati, Z. Liu and S. Gambhir, *Nat. Nanotechnol.*, 2008, **3**, 557-562.

13 G. Ku, M. Zhou, S. L. Song, Q. Huang, J. Hazle and C. Li, *ACS Nano* 2012, **6**, 7489-7496.

14 X. M. Yang, E. W. Stein, S. Ashkenazi and L. H. V. Wang, *Wiley Interdiscip Rev. Nanomed. Nanobiotechnol.*, 2009, **1**, 360-368.

15 C. Ginestier, S. Liu, M. E. Diebel, H. Korkaya, M. Luo and M. Brown, *J. Clin. Invest.*, 2010, 120, 485-497.

16 M. Zhou, R. Zhang, M. Huang, W. Lu, S. Song, M. P. Melancon and C. Li, *J. Am. Chem. Soc.*, 2010, **132**, 15351-15358.

17 K. Homan, S. Kim, Y. S. Chen, B. Wang, S. Mallidi and S. Emelianov, *Opt. Lett.*, 2010, **35**, 2663-2665.

18 A. P. Pathak, M. F. Penet, Z. M and Bhujwalla. *Adv. Genet.*, 2010, **69**, 1-30.

19 W. Cai, K. Chen, Z. B. Li, S. Gambhir and X. Chen, *J. Nucl. Med.*, 2007, **48**, 1862-1870.

20 R. R. Anderson and J. A. Parrish. *Science*, 1983, **220**, 524-527.

21 S. Peeters, M. Kitz, S. Preisser, A. Wetterwald, B. Rothen-Rutishauser and G. N. Thalmann, *Biomed. Opt. Express*, 2012, **3**, 435-446.

22 T. Ando, S. Sato, T. Toyooka, Y. Uozumi, H. Nawashiro and H. Ashida, *J. Biomed. Opt.*, 2011, **16**, 108002.

23 B. W. Barry, *Eur. J. Pharm. Sci.*, 2001, **14**, 101-114.

Fig 1.

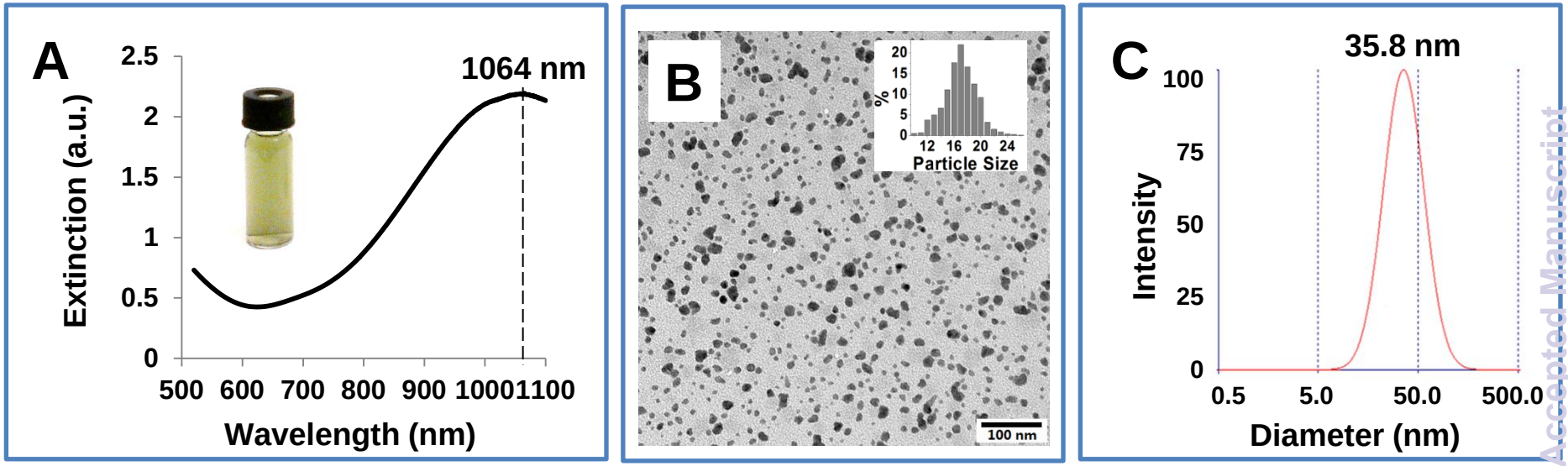

Fig 2.

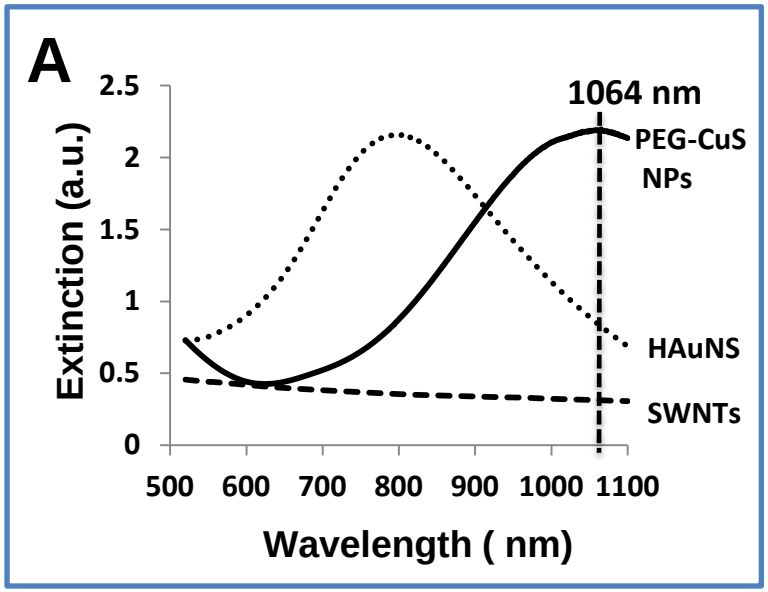

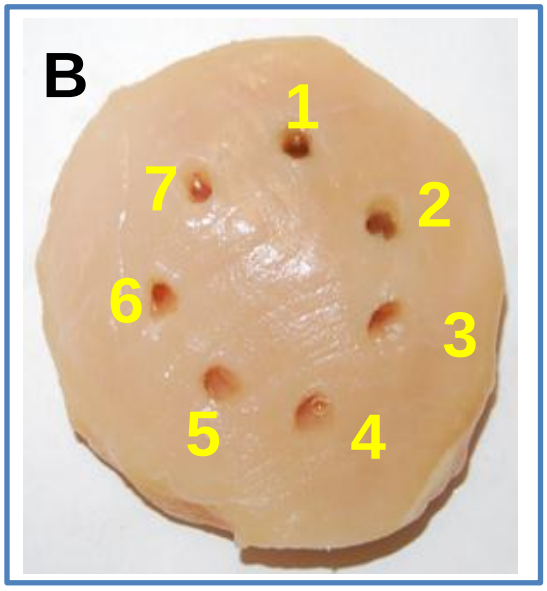

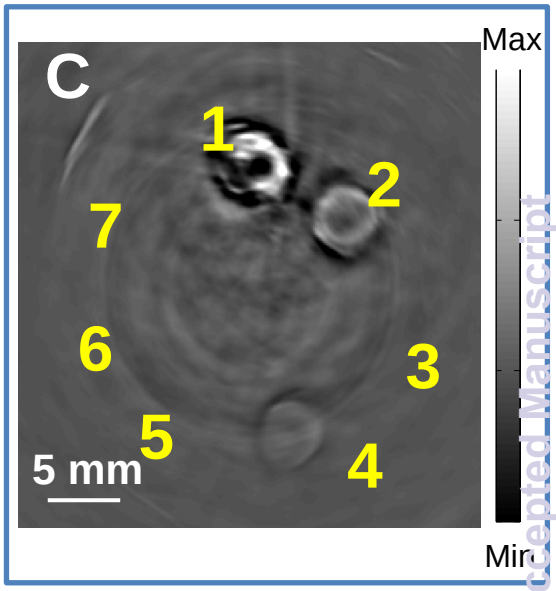

Fig 3.

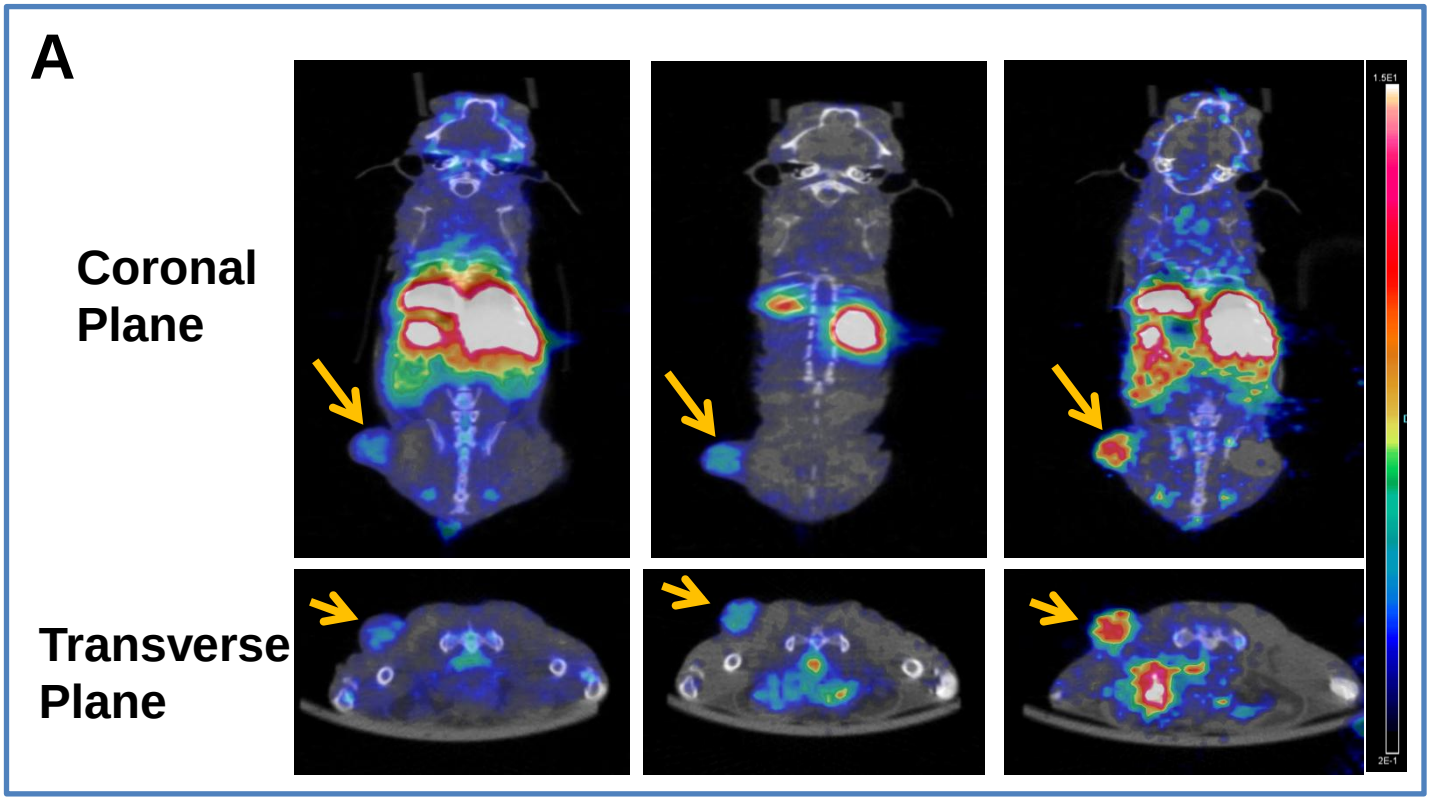

Fig 3.

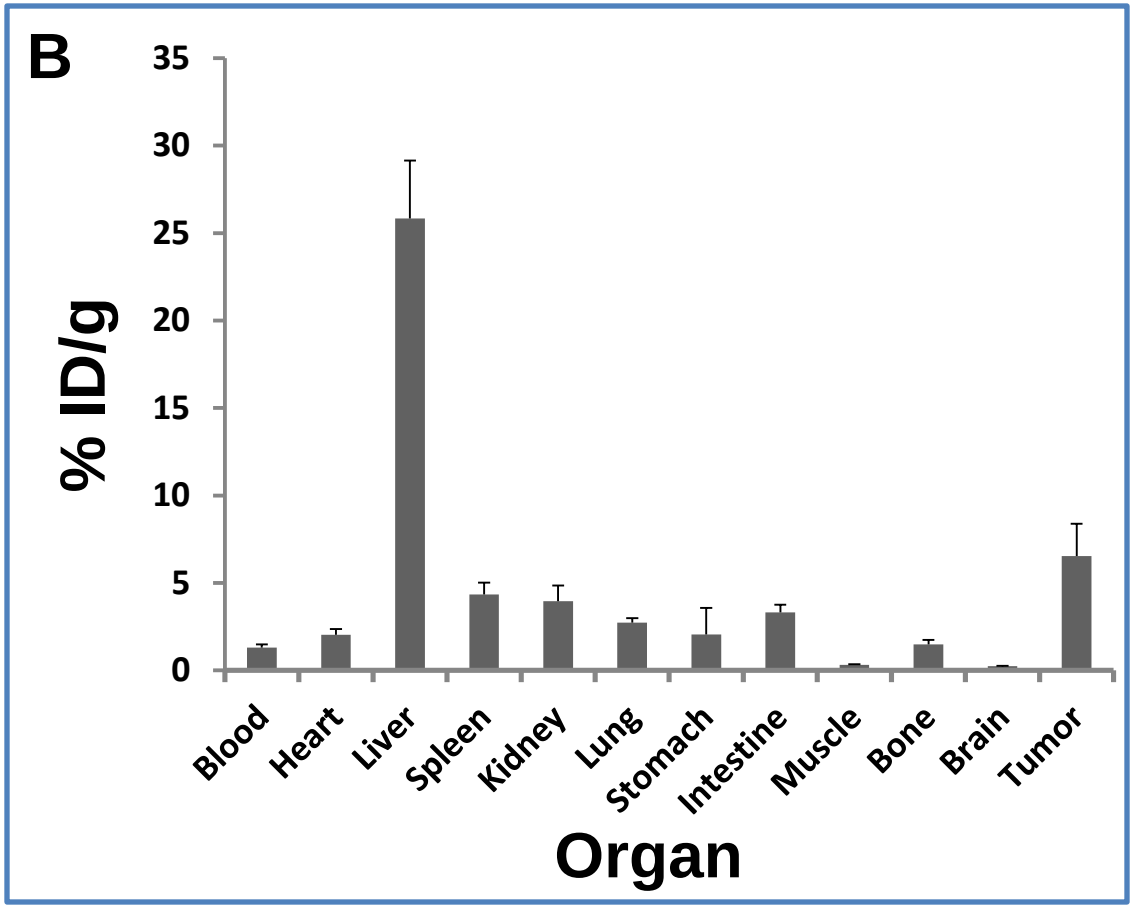

Fig 4.

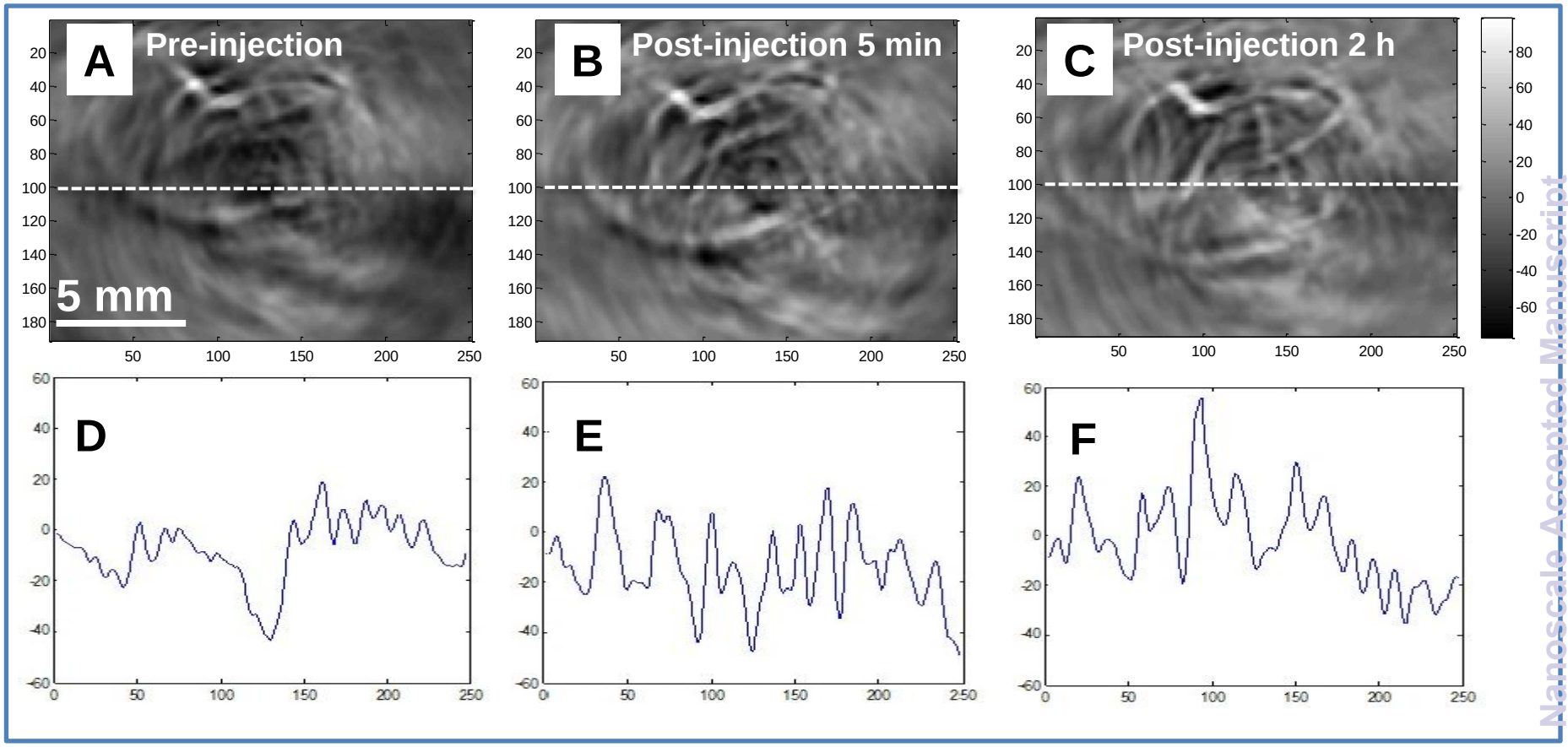

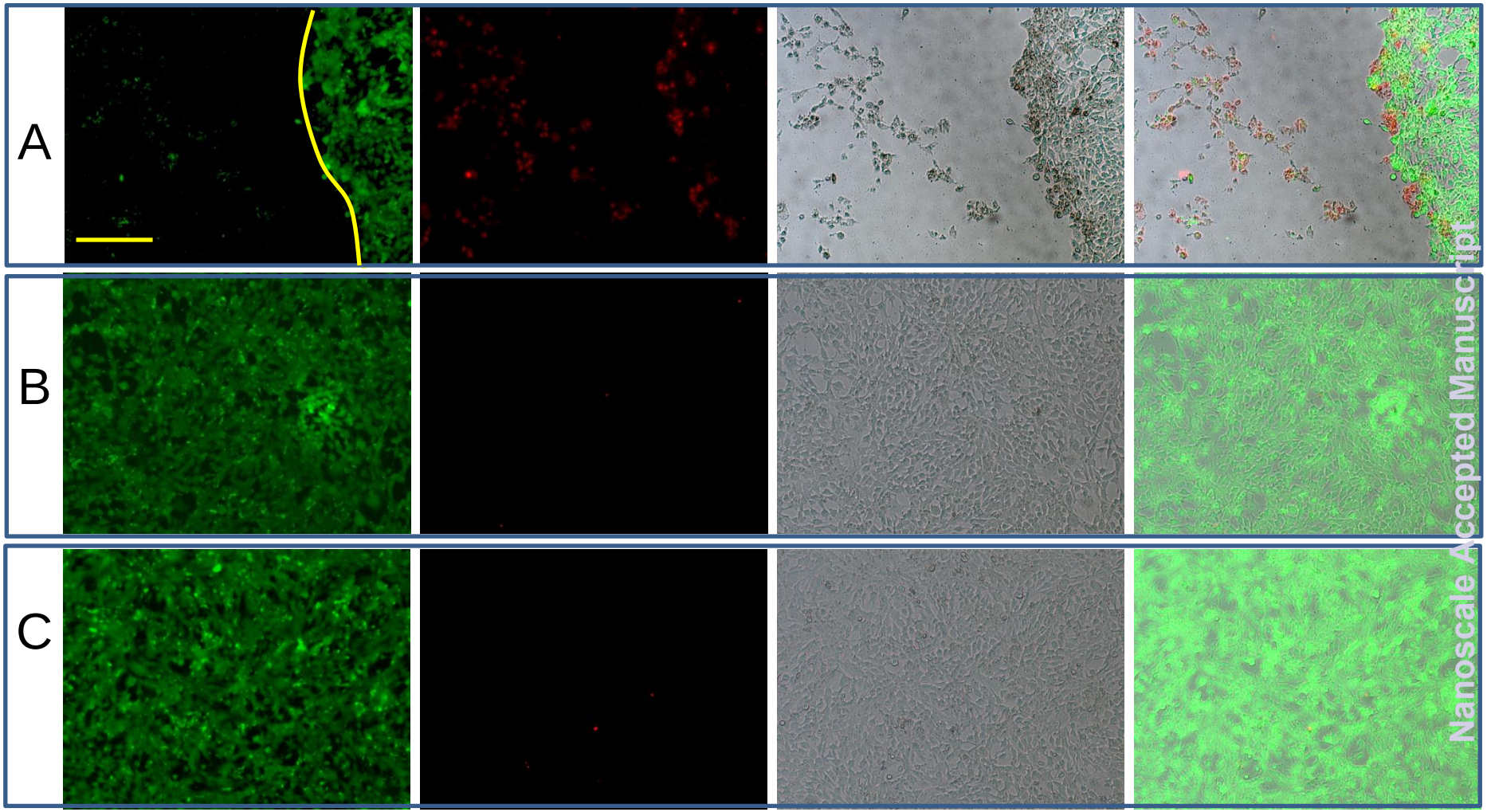

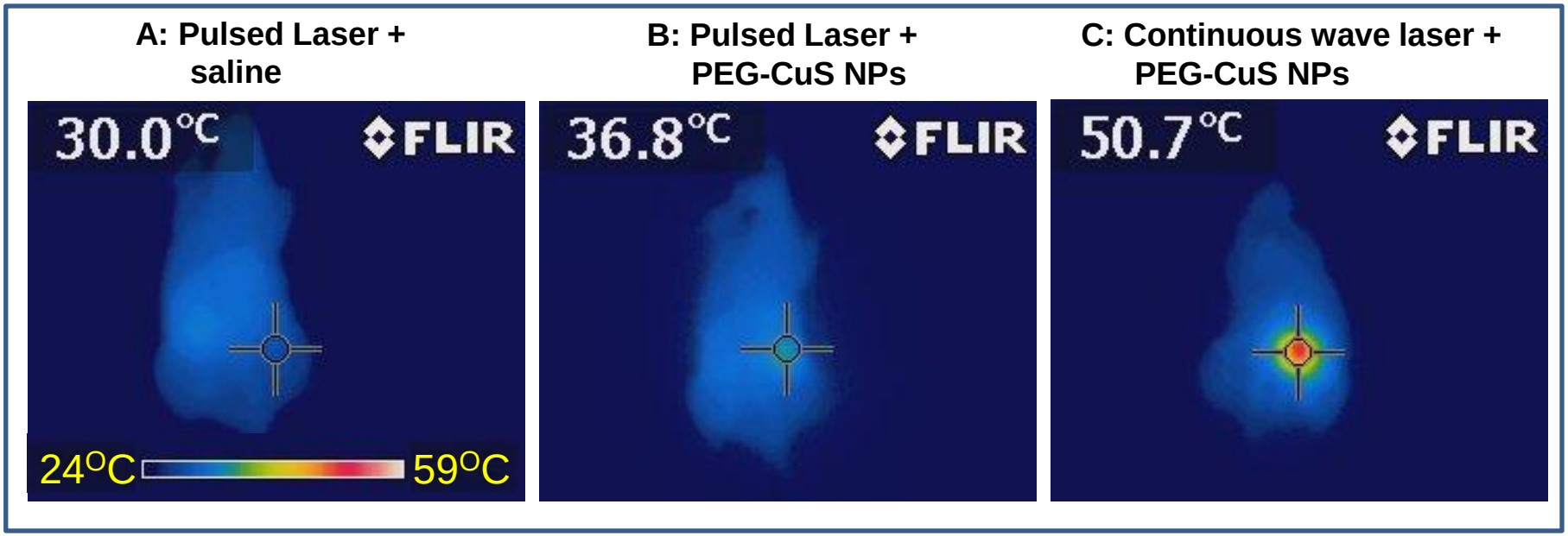

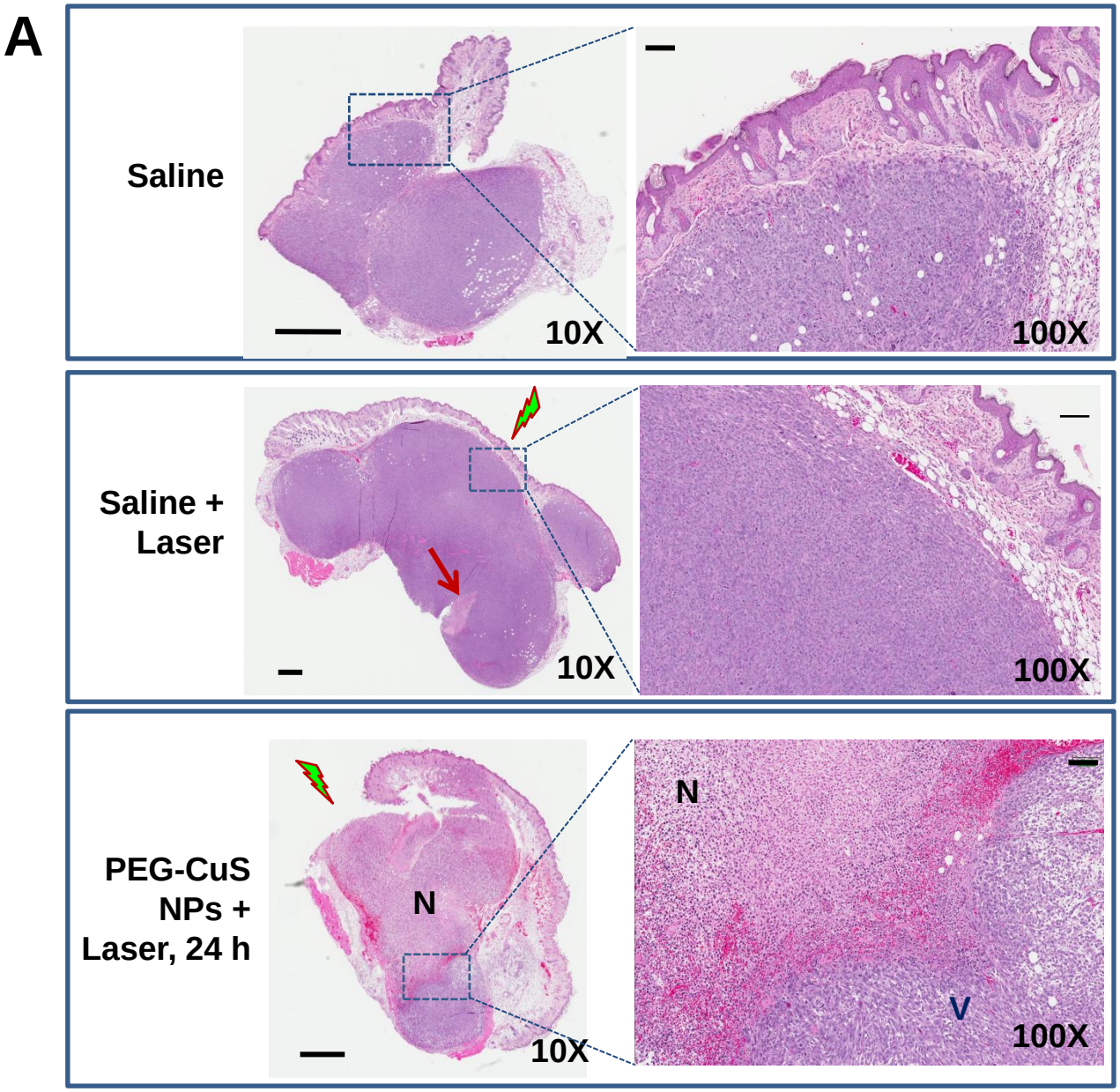

Fig 7.